Laser and Particle Beams (2016), *34*, 294–298.

doi:10.1017/S0263034616000136

Enhanced efficiency of femtosecond laser-driven proton generation from a two-species target with heavy atoms

J. DOMAŃSKI, J. BADZIAK, AND S. JABŁOŃSKI
Institute of Plasma Physics and Laser Microfusion, Hery 23, 01-497 Warsaw, Poland
(RECEIVED 21 December 2015; ACCEPTED 9 February 2016)

Abstract

Using two-dimensional particle-in-cell simulations, the properties of a proton beam generated from a thin erbium hydride target irradiated by a 25 fs laser pulse of intensity ranging from 10^{20} to 10^{21} W/cm^2 are investigated and compared with the features of a proton beam produced from a hydrocarbon (CH) target. It is shown that in case of using the hydride target the mean proton energy and the number of high-energy (>10 MeV) protons as well as the peak proton pulse intensity can be higher by a factor ~10 than the ones obtained from the CH target.

Keywords: Laser acceleration; Laser plasma; Ions; Particle-in-cell simulations

1. INTRODUCTION

The recent progress in laser technology has resulted in construction of short-pulse lasers generating picosecond or femtosecond pulses of powers in the sub-PW – PW range and intensities approaching 10^{22} W/cm^2 (Danson *et al.*, 2015). The interaction of such laser pulses with a solid target can result in the production of energetic ion beams with unique features, useful for research in various branches of physics, technology, and medicine, including nuclear physics (Ledingham & Galster, 2010), inertial confinement fusion (ICF) (Fernandez *et al.*, 2014), ion implantation (Torrisi *et al.*, 2003), or hadron cancer therapy (Bulanov *et al.*, 2002). Intense ion beams desirable for these applications can potentially be produced by several laser-induced ion acceleration mechanisms which are presently studied. They include the target normal sheath acceleration (TNSA) (Wilks *et al.*, 2001; Borghesi *et al.*, 2006; Badziak, 2007; Macchi *et al.*, 2013), the skin-layer ponderomotive acceleration (SLPA) (Badziak, 2007, 2008, 2011) [at high laser intensities, >10^{20} W/cm^2, this method is usually referred to as radiation pressure acceleration (Esirkepov *et al.*, 2004; Macchi *et al.*, 2005, 2013; Liseykina *et al.*, 2008; Robinson *et al.*, 2008)], the laser break-out afterburner (Yin *et al.*, 2006, 2007; Macchi *et al.*, 2013; Fernandez *et al.*, 2014), the collisionless electrostatic shock acceleration (Denavit, 1992; Silva *et al.*, 2004; Macchi *et al.*, 2013; Feranandez *et al.*, 2014), or the laser-induced cavity pressure acceleration (Badziak *et al.*, 2012, 2013). In a real experiment, two or even more acceleration mechanisms can contribute to the ion acceleration process and the dominated one depends on both the laser pulse and target parameters. These parameters also determine characteristics of generated ion beams. The effect of laser pulse intensity, duration, and polarization as well as the target thickness on properties of the ion beams was studied in numerous papers (see, e.g., Macchi *et al.*, 2005, 2013; Borghesi *et al.*, 2006; Robson *et al.*, 2007; Liseykina *et al.*, 2008) both numerically and experimentally. However, the influence of target composition on these properties has been investigated to a much lesser degree (e.g. Foord *et al.*, 2008; Davis & Petrov, 2009; Cui *et al.*, 2013; Liu *et al.*, 2013; Domański *et al.*, 2014; Weng *et al.*, 2015), in spite of the fact that optimally selected target composition can potentially lead to a significant enhancement in ion beam parameters. In particular, this issue is of high importance for optimized generation of proton beams from hydrogen-rich multi-species targets.

In this paper, the effect of target composition on laser-driven proton generation from hydrogen-rich targets is investigated using a two-dimensional (2D), relativistic particle-in-cell (PIC) code. The properties of a proton beam generated from a thin hydride target with heavy atoms [erbium hydride (ErH_3)] irradiated by a femtosecond laser pulse emitted from a petawatt-class Ti-sapphire laser are compared with the properties of a proton beam produced from a commonly used hydrocarbon (CH) target. It is shown that in case of using the hydride target the peak and the mean proton energies, the

Address correspondence and reprint requests to: J. Domański, Institute of Plasma Physics and Laser Microfusion, Hery 23, 01-497 Warsaw, Poland. E-mail: jaroslaw.domanski@ifpilm.pl

number of high-energy protons as well as the proton beam intensity can be considerably higher than the ones obtained from the CH target.

2. RESULTS AND DISCUSSION

The numerical simulations were performed for a linearly polarized laser pulse of 25 fs duration [full-width at half-maximum (FWHM)], intensity ranging from 10^{20} to 10^{21} W/cm^2 and 800 nm wavelength. The laser pulse shape in time and space (along the *y*-axis) was described by a super-Gaussian function of the form $\exp(-t/t_0)^6(-y/y_0)^6$ and the laser beam width (FWHM) was assumed to be 8 μm. The laser pulse interacted with the ErH_3 or the CH target of the transverse dimension of 12 μm and of the areal mass density same for both targets and equal to 0.06 mg/cm^3. Molecular densities of the targets corresponded to solid-state densities and they were equal to 4.86×10^{22} molecules/cm^3 for CH and 2.69×10^{22} molecules/cm^3 for ErH_3. The ionization degrees of targets' components were assumed to be 1 for hydrogen, 6 for carbon, and 10 for erbium (Davis & Petrov, 2009). In front of the target, a pre-plasma layer of 0.25 μm thickness and the density shape described by an exponential function was placed. The 2D relativistic PIC code used for the simulations was an extended version (two dimensions in particle densities and three dimensions in particle velocities and fields) of our one-dimensional PIC code (Badziak & Jabłoński, 2010) which, in turn, was a modified version of a well-known LPIC++ code (Lichters *et al.*, 1997). The simulations were performed in the *s, y* space equal to 80×32 μm^2 and the number of macroparticles (optimized) was assumed to be 5×10^6.

Figure 1 presents 2D spatial profiles of charge density for Er ions and protons generated from the ErH_3 target by the laser pulse of intensity $I_L = 10^{21}$ W/cm^2 at time $t = 0.4$ ps when the proton peak energy approaches its maximum value ($t = 0$ corresponds to the moment when the pulse starts to interact with the pre-plasma layer at the target front placed at $s = 1.25$ μm). It can be seen that almost all protons stored in the target are accelerated to high velocities ($>10^9$ cm/s) and are clearly separated from the erbium ions which attain much lower velocities and most of these ions are concentrated close to the target's initial position. The 2D spatial profiles of charge density for C ions and protons produced from the CH target at $I_L = 10^{21}$ W/cm^2 and $t = 0.4$ ps are presented in Figure 2. In this case, both protons and carbon ions are accelerated to high velocities and most of them move together. There are clearly seen two groups of protons of different proton energies and majority of protons is stored in the low-energy group. Moreover, the protons are more dispersed in space and the proton beam is less collimated than in the case of ErH_3 target (Fig. 1b).

Figure 3 presents the integrated energy spectra of protons, generated forward from ErH_3 or CH targets at $I_L = 10^{21}$ W/cm^2, for the intermediate ($t = 0.1$ ps) and the final ($t = 0.4$ ps) stage of the proton acceleration (the spectra are integrated over the whole *y, s* space assumed for the simulations). For both acceleration stages, the peak and the mean energy of protons generated from the ErH_3 target are clearly higher than those produced from

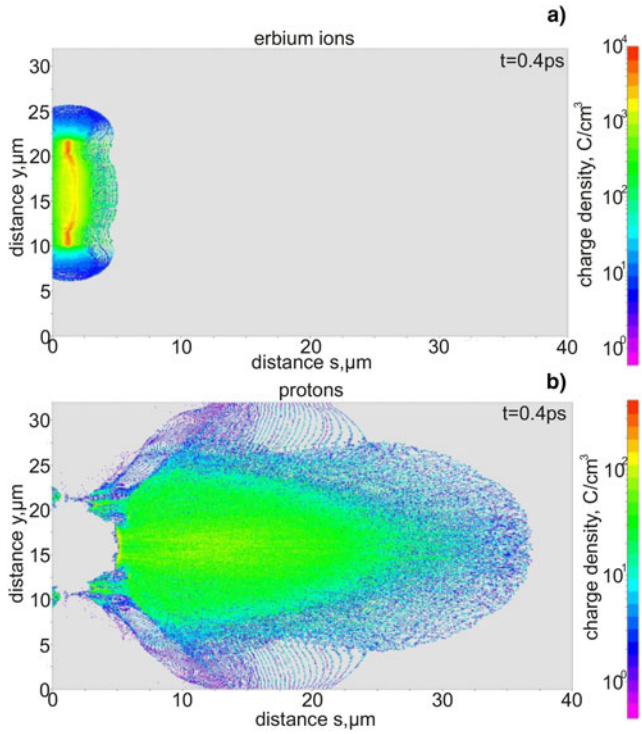

Fig. 1. 2D spatial distributions of charge density of erbium ions (a) and protons (b) generated from the ErH_3 target. $I_L = 10^{21}$ W/cm^2.

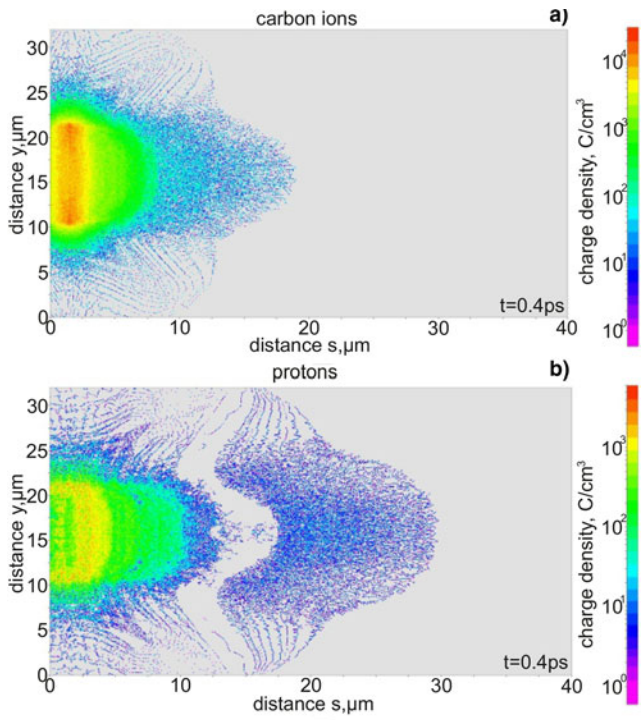

Fig. 2. 2D spatial distributions of charge density of carbon ions (a) and protons (b) generated from the CH target. $I_L = 10^{21}$ W/cm^2.

https://doi.org/10.1017/S0263034616000136 Published online by Cambridge University Press

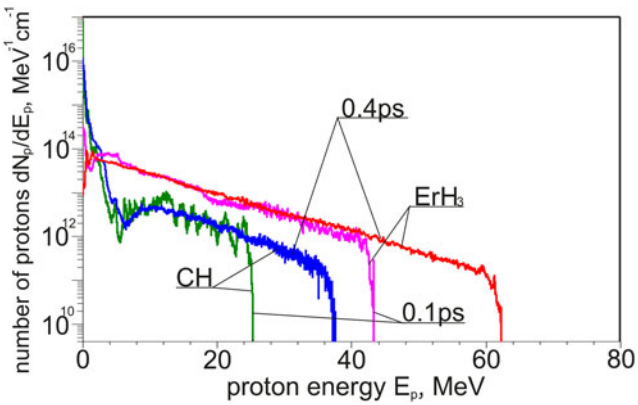

Fig. 3. The energy spectra of protons generated forward from the ErH_3 target and the CH target for two different stages of the proton acceleration. $I_L = 10^{21}$ W/cm^2.

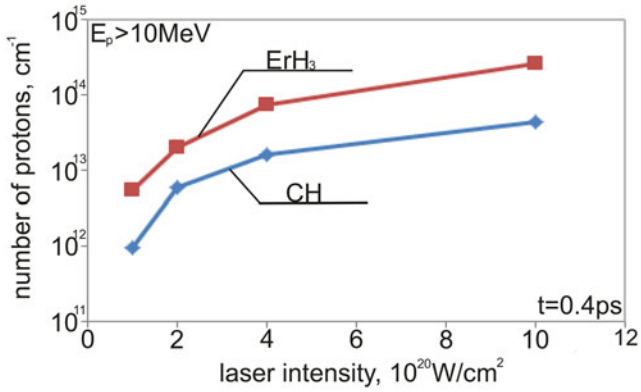

Fig. 5. The number of high-energy (>10 MeV) protons generated from the ErH_3 target and the CH target as a function of the laser pulse intensity.

the CH target and, moreover, the number of low-energy protons in the first case is much lower than in the CH target case (it is consistent with what can be concluded from a comparison of Figs 1b and 2b).

The quantitative values of the peak and the mean proton energies as well as the number of high-energy ($E_p > 10$ MeV) protons for the ErH_3 and the CH targets, as a function of the laser pulse intensity, are shown in Figures 4 and 5 The peak proton energies are by a factor ~1.5–2 higher for ErH_3 than for CH; however, the mean proton energies are by a factor ~10 higher for ErH_3 and they are in the multi-MeV range (for $I_L \geq 2 \times 10^{20}$ W/cm^2), while for CH the mean energies are below 1 MeV. A difference between the numbers of high-energy protons generated from ErH_3 and CH is also large and for the ErH_3 target this number is nearly an order of magnitude higher than for the CH target (Fig. 5). Moreover, while in case of ErH_3 more than 30% of the total amount of protons stored in the target is accelerated to energies >10 MeV at $I_L = 10^{21}$ W/cm^2, only ~1% of protons stored in the CH target is accelerated to such energies.

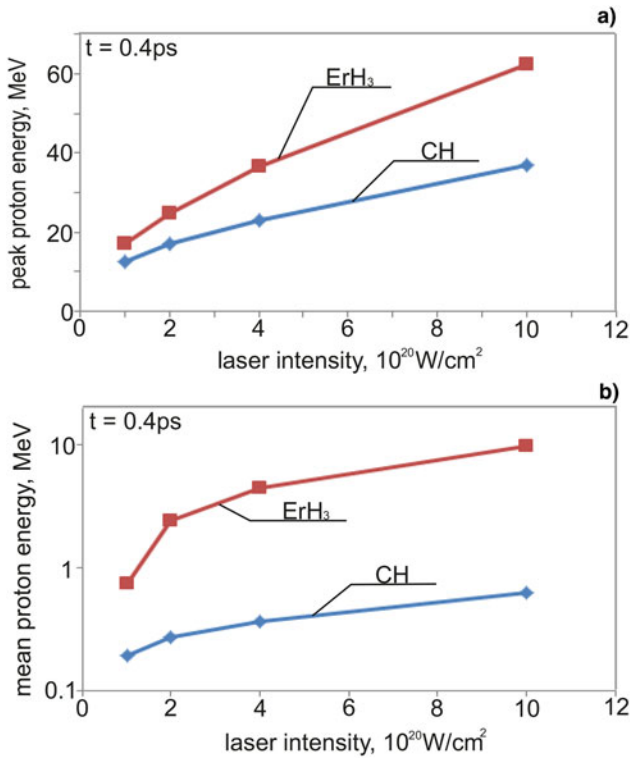

Fig. 4. The peak energy (a) and the mean energy (b) of protons generated from the ErH_3 target and the CH target as a function of the laser pulse intensity.

The effect of interaction of ion beam with any object irradiated by the beam is determined not only by the ion energies, but also by other characteristics of the beam, in particular by the ion beam intensity $I_i = n_i v_i E_i$ (n_i, v_i, E_i are the ion density, the ion velocity, and the ion energy, respectively). A high ion beam intensity is desirable for various ion beam applications in high energy-density physics and nuclear physics as well as in some technological applications (Torrisi *et al.*, 2003; Ledingham & Galster, 2010; Fernandez *et al.*, 2014). Important characteristics are also the ion pulse duration and the pulse shape. Very short (ps scale) ion pulses are required for example for ICF fast ignition (Fernandez *et al.*, 2014), isochoric heating of matter (Patel *et al.*, 2003), or proton radiography (Borghesi *et al.*, 2006). Figure 6 presents a comparison of proton pulses (the temporal runs of proton beam intensity averaged over $\Delta y = 16$ μm) produced from the ErH_3 and CH targets at $I_L = 10^{21}$ W/cm^2 and recorded in a close vicinity of the rear target surface ("at the source", Fig. 6a) and 5 μm behind this surface (Fig. 6b). In case of the ErH_3 target, the proton pulse duration "at the source" is close to the laser pulse duration (~25 fs) and its peak intensity is fairly high, above 2×10^{19} W/cm^2. The proton pulse generated from the CH target is much longer (~90 fs) and its peak intensity is by an order of magnitude lower than for ErH_3. Due to the proton velocity dispersion the proton pulse length increases with an increase in the distance from the target and, as a result, the proton pulse intensity decreases. However, in case of ErH_3 the proton pulse shape does not change significantly (it remains a

https://doi.org/10.1017/S0263034616000136 Published online by Cambridge University Press

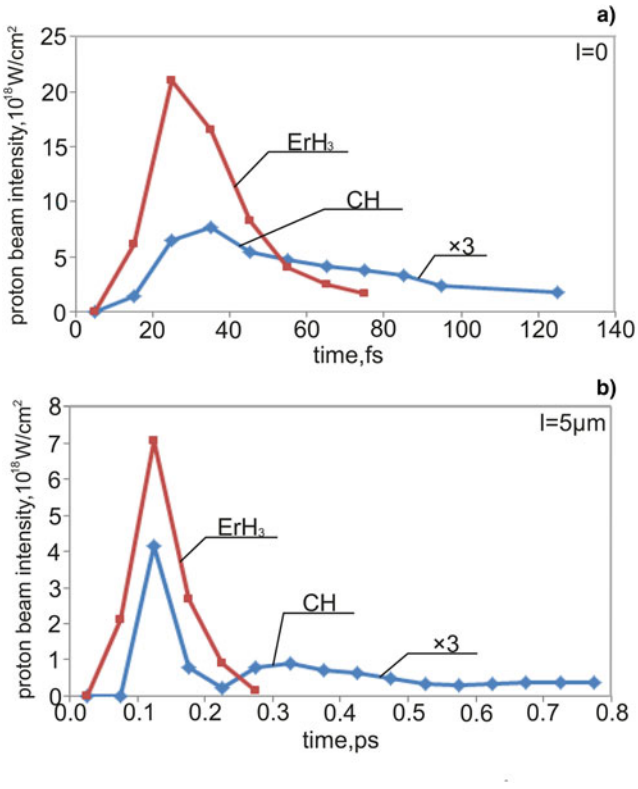

Fig. 6. The proton pulses produced from the ErH_3 target and the CH target and recorded in a close vicinity of the rear target surface (a) and 5 μm behind this surface (b). $I_L = 10^{21}$ W/cm^2. Note that the proton beam intensities for the CH target are magnified be the factor 3 in the figure.

"mono-pulse"), while in case of CH a double-pulse structure, with the high-energy and low-energy proton groups is revealed during the proton pulse propagation. This picture is consistent with that revealed by the 2D proton charge distribution in Figure 2b, where two proton groups of different energies are clearly seen. Thus, the ErH_3 target allows not only attaining higher proton energies than those attainable with the CH target but also obtaining significantly more intense and compact proton pulse.

The observed differences between energies and intensities of proton beams generated using CH and ErH_3 can be explained by the difference in the strength of interaction between heavier ions (Er, C) stored in the target and the electric field, induced by laser in plasma, which accelerates these ions. This interaction depends on the q/m parameter (q is the ion charge, and m is the ion mass) which is much smaller for erbium ions than for carbon ions. As a result, the interaction between erbium ions and the field is much weaker than the interaction between the field and carbon ions. For this reason amount of energy transferred by the field to protons in the erbium–hydrogen plasma is higher than in the CH plasma. The high erbium ion mass is also a main reason for the observed separation between erbium ions and protons (Fig. 1).

A detailed analysis of spatial distributions of ion and electron densities as well as electric fields in plasma and their evolution in time shows that for both targets considered the process of ion acceleration is fairly complex and both TNSA- and SLPA-like mechanisms contribute to this process, though in the late phase of acceleration ($t \geq 100$ fs) the TNSA-like mechanism dominates. Both protons and heavier ions are accelerated by the electric field produced due to a separation of electrons – accelerated by the laser-induced ponderomotive forces – from the ions. A majority of electrons is pushed by these forces forward, mainly in the direction close to the laser beam axis and, as a result, the charge separation electric field, which accelerates ions, is also directed mostly close to this axis. The spatial structure of the field is complex and changes in time; however, in the late phase of acceleration two peaks (usually with a substructure) can be distinguished in this structure: the first one placed relatively close to the target's rear surface and the second one situated far behind the rear surface. This double-peak structure of the field is observed for both considered target types and in case of ErH_3 it is responsible for the separation of protons from erbium ions (Fig. 1), while in case of CH it is the main reason for the two groups of protons observed: the high-energy proton group accelerated separately from carbon ions and the low-energy group accelerated together with these ions (Fig. 2). However, the strength and detailed structure of the accelerating fields are different for both targets and, as a result, parameters of the proton and ion beams generated from these targets are also different (as it was demonstrated in the early presented figures).

3. CONCLUSIONS

In conclusion, it has been shown that using hydride targets with heavy atoms, instead of commonly used CH targets, allows a considerable increase in all practically important parameters of the femtosecond laser-generated proton beams. In particular, the application of a thin ErH_3 target for the proton production can result in an increase in the mean proton energy, the peak proton pulse intensity and the number of multi-MeV protons even by an order of magnitude as compared with the case when a CH target is used. Since high-power femtosecond lasers are generally capable of working with a high repetition rate (>1 Hz) (Danson *et al.*, 2015), the demonstrated increase in the efficiency of multi-MeV proton generation using such lasers can be considered as a significant step toward broadening the range of applications of laser-driven proton beams which are practically feasible with currently available lasers.

ACKNOWLEDGEMENTS

This work was supported in part by the National Science Centre (NCN), Poland under the Grant no. 2014/14/M/ST7/00024; and the simulations was carried out with the support of the Interdisciplinary Centre for Mathematical and Computational Modelling (ICM), University of Warsaw under Grant no. G57-20.

https://doi.org/10.1017/S0263034616000136 Published online by Cambridge University Press

REFERENCES

Badziak, J. (2007). Laser-driven generation of fast particles. *Opto-Electron. Rev.* **15**, 1.

Badziak, J. & Jabłoński, S. (2010). Ultraintense ion beams driven by a short-wavelength short-pulse laser. *Phys. Plasmas* **17**, 073106.

Badziak, J., Jabłoński, S., Parys, P., Rosiński, M., Wołowski, J., Szydłowski, A., Antici, P., Fuchs, J. & Mancic, A. (2008). Ultraintense proton beams from laser-induced skin-layer ponderomotive acceleration. *J. Appl. Phys.* **104**, 063310.

Badziak, J., Jabłoński, S., Pisarczyk, T., Rączka, P., Krousky, E., Liska, R., Kucharik, M., Chodukowski, T., Kalinowska, Z., Parys, P., Rosiński, M., Borodziuk, S. & Ullschmied, J. (2012). Highly efficient accelerator of dense matter using laser-induced cavity pressure acceleration. *Phys. Plasmas* **19**, 053105.

Badziak, J., Mishra, G., Gupta, N.K. & Holkundkar, A.R. (2011). Generation of ultraintense proton beams by multi-ps circularly polarized laser pulses for fast ignition-related applications. *Phys. Plasmas* **18**, 053108.

Badziak, J., Parys, P., Rosiński, M., Krousky, E., Ullschmied, J. & Torrisi, L. (2013). Improved generation of ion fluxes by a long laser pulse using laser-induced cavity pressure acceleration. *Appl. Phys. Lett.* **103**, 124104.

Borghesi, M., Fuchs, J., Bulanov, S.V., Mackinnon, A.J., Patel, P.K. & Roth, M. (2006). Fast ion generation by high-intensity laser irradiation of solid targets and applications. *Fusion Sci. Technol.* **49**, 412.

Bulanov, S.V., Esirkepov, T.Zh., Khoroshkov, V.S., Kuznetsov, A.V. & Pegoraro, F. (2002). Oncological hadrontherapy with laser ion accelerators. *Phys. Lett.* A **299**, 240.

Cui, Y.-Q., Wang, W.-M., Sheng, Z.-M., Li, Y.-T. & Zhang, J. (2013). Quasimonoenergetic proton bunches generation from doped foil targets irradiated by intense lasers. *Phys. Plasmas* **20**, 024502.

Danson, C., Hillier, D., Hopps, N. & Neely, D. (2015). Petawatt class lasers worldwide. *High Power Laser Sci. Eng.* **3**, e3.

Davis, J. & Petrov, G.M. (2009). Generation of GeV ion bunches from high-intensity laser-target interactions. *Phys. Plasmas* **16**, 023105.

Denavit, J. (1992). Absorption of high-intensity subpicosecond lasers on solid density targets. *Phys. Rev. Lett.* **69**, 3052.

Domański, J., Badziak, J. & Jabłoński, S. (2014). Particle-in-cell simulation of acceleration of ions to GeV energies in the interactions of an ultra-intense laser pulse with two-species targets. *Phys. Scr.* **T161**, 014030.

Esirkepov, T., Borghesi, M., Bulanov, S.V., Mourou, G. & Tajima, T. (2004). Highly efficient relativistic-ion generation in the laser-piston regime. *Phys. Rev. Lett.* **92**, 175003.

Fernandez, J.C., Albright, B.J., Beg, F.N., Foord, M.E., Hegelich, B.M., Honrubia, J.J., Roth, M., Stephens, R.B. & Yin, L. (2014). Fast ignition with laser-driven proton and ion beams. *Nucl. Fusion* **54**, 054006.

Foord, M.E., Mackinnon, A.J., Patel, P.K., MacPhee, A.G., Ping, Y., Tabak, M. & Town, R.P.J. (2008). Enhanced proton production from hydride-coated foils. *J. Appl. Phys* **103**, 056106.

Ledingham, K.W.D. & Galster, W. (2010). Laser-driven particle and photon beams and some applications. *New. J. Phys.* **12**, 045005.

Lichters, R., Pfund, R.E.W. & Meyer-Ter-Vehn, J. (1997). LPIC++: A parallel one-dimensional relativistic electromagnetic particle-cell-code for simulating laser-plasma-interactions. Report MPQ 225. Germany, Garching: Max-Planck-Institut für Quantenoptik. (the code is available at http://www.lichters.net/download.html).

Liseykina, T.V., Borghesi, M., Macchi, A. & Tuveri, S. (2008). Radiation pressure acceleration by ultraintense laser pulses. *Plasma Phys. Control. Fusion* **50**, 124033.

Liu, T.-C., Shao, X., Liu, C.-S., He, M., Eloasson, B., Tripathi, V., Su, J.-J., Wang, J. & Chen, S.-H. (2013). Generation of quasi-monoenergetic protos from thin multi-ion foils by a combination of laser radiation pressure acceleration and shielded Coulomb repulsion. *New J. Phys.* **15**, 025026.

Macchi, A., Borghesi, M. & Passoni, M. (2013). Ion acceleration by superintense laser-plasma interaction. Rev. *Mod. Phys.* **85**, 751.

Macchi, A., Cattani, F., Liseykina, T.V. & Cornalti, F. (2005). Laser acceleration of ion bunches at the front surface of overdense plasmas. *Phys. Rev. Lett.* **94**, 165003.

Patel, P.K., MacKinnon, A.J., Key, M.H., Cowan, T.E., Foord, M.E., Allen, M., Price, D.F., Ruhl, H., Springer, P.T. & Stephens, R. (2003). Isochoric heating of solid-density matter with an ultrafast proton. *Phys. Rev. Lett.* **91**, 125004.

Robinson, A.P.L., Zepf, M., Kar, S., Evans, R.G. & Bellei, C. (2008). Radiation pressure acceleration of thin foil with circular polarized laser pulse. *New J. Phys.* **10**, 013021.

Robson, L., Simpson, P.T., Clarke, R.J., Ledingham, K.W.D., Lindau, F., Lundh, O., McCanny, T., Mora, P., Neely, D., Wahlstrom, C.G., Zepf, M. & McKenna, P. (2007). Scaling of proton acceleration driven by petawatt-laser–plasma interactions. *Nat. Phys.* **3**, 58.

Silva, L.O., Marti, M., Davies, J.R. & Fonseca, R.A. (2004). Proton shock acceleration in laser–plasma interactions. *Phys. Rev. Lett.* **92**, 015002.

Torrisi, L., Gamino, S., Mezzasalma, A.M., Badziak, J., Parys, P., Wolowski, J., Woryna, E., Krasa, J., Laska, L., Pfeifer, M., Rohlena, K. & Boody, F.P. (2003). Implantation of ions produced by the use of high power iodine laser. *Appl. Surf. Sci.* **217**, 319.

Weng, S.M., Murakami, M. & Sheng, Z.M. (2015). Reducing ion energy spread in hole-boring radiation pressure acceleration by using two-ion-species targets. *Laser Part. Beams* **33**, 103–107. doi: 10.1017/S026303461400069X.

Wilks, S.C., Langdon, A.B., Cowan, T.E., Roth, M., Singh, M., Hatchett, S., Key, M.H., Pennington, D., MacKinnon, A. & Snavely, R.A. (2001). Energetic proton generation in ultra-intense laser–solid interactions. *Phys. Plasmas* **8**, 542.

Yin, L., Albright, B.J., Hegelich, B.M., Browers, K.J., Flippo, K.A., Kwan, T.J.T. & Fernandez, J.C. (2007). Monoenergetic and GeV ion acceleration from the laser breakout afterburner using ultrathin targets. *Phys. Plasmas* **14**, 056706.

Yin, L., Albright, B.J., Hegelich, B.M. & Fernandez, J.C. (2006). GeV laser ion acceleration from ultrathin targets: The laser break-out afterburner. *Laser Part. Beams* **24**, 291–298. doi: 10.1017/S0263034606060459.